Electronic Supplementary Information (ESI) for

A High-Performance Highly-Bendable Quasi-Solid-State Zinc-Organic Battery Enabled by Intelligent Proton-Self-Buffering Copolymer Cathodes

Ping Li, [§a] Zhengsong Fang, [§a] You Zhang, [§a] Chunshao Mo,[a] Xuanhe Hu,[a] Junhua Jian,[a] Shuangyin Wang[b] and Dingshan Yu*[a]

[a] Key Laboratory for Polymeric Composite and Functional Materials of Ministry of Education, School of Chemistry, Sun Yat-sen University, Guangzhou 510275, China

[b] *State Key Laboratory of Chem/Bio-Sensing and Chemometrics, College of Chemistry and Chemical Engineering, Hunan University, Changsha 410082, China.*

Experimental section

***Preparation of carbon cloth-porous carbon (CC-PC) conductive scaffold*:** Polystyrene (PS) spheres as the template was prepared according to previous reports.[1] Typically, a 500-mL of two-necked flask was charged with 0.1 g of ammonium persulfate, 0.12 g of Na_2CO_3, 5 mL of styrene, 0.5 mL of acrylic acid and 100 mL of deionized water (DI) under inert N_2 protection. The reaction was kept at 70 °C for 7 h to generate white suspension, followed by the centrifugation at 8000 rpm for 5 mins and subsequent extensive washing with DI water. The obtained white solid was ultrasonically dispersed in 100 mL of DI water. Afterwards, a piece of carbon cloth was subjected to electrochemical treatment successively in 1 M H_2SO_4 for 3 h at a constant voltage of 2 V, followed by repeated rinsing with ethanol and DI water and vacuum drying at 60 °C. The treated carbon cloth was cut into pieces of 1 x 5 cm^{-2} and placed vertically into a vial containing 9 mL of PS dispersion. Afterwards, the loaded vial was put in a temperature- and humidity-controlled chamber with the temperature of 65 °C and the relative humidity of 75 % for 2-3 days for generating the opal structure assembled on CC. The CC anchored with the opal structure was impregnated in an aqueous solution of cube sugar (0.06 M) and H_2SO_4 (0.025 M). After subjecting to heat-treatment at 100 °C for 6 h, the CC turned brown and was subsequently transferred to an empty glass bottle in an oven with the temperature at 150 °C for 6 h. Finally, the CC-PC was obtained by the calcination of the above CC at 650 °C for 2 h, and 800 °C for another 2 h in a N_2 steam.

***Preparation of CC-PC@PANAC Cathode*:** The poly (aniline-co-Azure C) (PANAC) was conformally assembled onto the CC-PC scaffold by the electrochemical copolymerization using a CHI 760e electrochemical workstation with CC-PC as the working electrode, the Pt foil as the counter electrode and the saturated calomel electrode (SCE) as the reference electrode. Cyclic voltammetry (CV) was conducted in an aqueous solution consisting of 0.2 M aniline, 2.5 mM Azure C (AC) and 0.5 M H_2SO_4 in a potential range of –0.20 to 1.10 V at a scan rate of 60 mV s^{-1} for 50 cycles. After the copolymerization, the PANAC films were grown on the CC-PC substrate. The obtained CC-PC@PANAC was rinsed with DI water and dried at 60 °C in

vacuum. The mass loading of PANAC on CC-PC can be regulated by varying polymerization time. The optimal mass loading of PANAC was 3.6 mg cm^{-2} for achieving the best electroactivity.

***Preparation of CC-PC@PANI Cathode*:** The poly (aniline) (PANI) was conformally assembled onto the CC-PC scaffold by the electrochemical copolymerization using a CHI 760e electrochemical workstation with CC-PC as the working electrode, the Pt foil as the counter electrode and SCE as the reference electrode. CV was conducted in an aqueous solution containing 0.2 M aniline and 0.5 M H_2SO_4 in a potential range of -0.20 to 1.10 V at a scan rate of 60 mV s^{-1} for 50 cycles. The mass loading of PANI on CC-PC can be regulated by varying polymerization time.

***Preparation of CC@Zn NP Anode*:** Zn electrodeposition was performed on a CHI 760e workstation with a piece of CC (1 cm × 2 cm) as the working electrode, the Pt foil as the counter electrode and SCE as the reference electrode. Typically, cathode pulse (-40 mA cm^{-2}, 10 s on, 6 s off, 25 mins) deposition method was applied in 100 mL of aqueous solution containing 12.5 g of zinc sulfate ($ZnSO_4 \cdot 7H_2O$), 12.5 g of sodium sulfate (Na_2SO_4) and 2 g of boric acid (H_3BO_3) at room temperature. The mass loading of CC@Zn NP can be readily adjusted by controlling the electrodeposition time. The optimal Zn mass loading on CC is 16.35 mg cm^{-2}.

***Materials Characterization*:** The morphology and microstructure of samples were examined on scanning electron microscope (SEM; Hitachi, S-4800), scanning electron microscopy-energy dispersive X-ray spectroscopy (SEM-EDX) and transmission electron microscopy (TEM, FEI Tecnai G^2 F30). The crystal structures of samples were assessed on X-ray power diffractometer (XRD, Rigaku D/Max2550, Cu Kα radiation) at room temperature. The Fourier transform infrared (FT-IR) spectra were recorded on a Thermal-Nicolet Nexus 670 spectrophotometer. UV-visible spectra of samples were carried out using an UV-2501PC spectrometer. The chemical state and compositions of samples were recorded on X-ray photoelectron

spectroscopy (XPS, ESCALab250).

***Fabrication of Quasi-Solid-State Zn-PANAC Battery*:** The quasi-solid-state Zn-PANAC battery was assembled with the CC-PC@PANAC cathode, the NKK separator, (Nippon Kodoshi Corporation), the CC@Zn NP anode and the PVA/NH_4Cl-$ZnCl_2$ gel electrolyte. PVA/NH_4Cl-$ZnCl_2$ gel electrolyte was produced as follows: 3 M NH_4Cl, 2 M $ZnCl_2$ and PVA (8.5 g) was mixed in 100 mL of DI water, and the mixture solution was heated to 85 °C under vigorous stirring until it became clear. Two electrodes (1 cm^2) were immersed in the gel electrolyte for 5 min and then dried until the gel solidification under ambient conditions. The mechanically robust quasi-solid-state Zn-conductive polymer cell was packed for subsequent tests.

***Electrochemical Measurements*:** The electrochemical measurements including CV, glvanostatic charge-discharge (GCD) curves, and electrochemical impedance spectroscopy were conducted on a CHI 760E electrochemical workstation with the sample as the working electrode, the Pt foil as the counter electrode and SCE as the reference electrode. The electrochemical characterization of two-electrode aqueous Zn-PANAC batteries was carried out at room temperature in an aqueous solution containing 3 M NH_4Cl and 2 M $ZnCl_2$ (pH = 5). According to previous reports,[2] The specific capacity (C_m, mAh g^{-1}) was calculated according to the following formula:

$$C_m = \frac{\int_0^{\Delta t} I \times dt}{m} \qquad (1)$$

where C_m is the specific capacity of the Zn-PANAC battery, Δt (h) is the discharge time, I (mA) is the discharge current during GCD and the m (g) is the mass of the active material of PANAC cathode.

The areal capacity (C_s, mAh cm^{-2}) was calculated from the discharge curve using the following equations:

$$C_s = \frac{\int_0^{\Delta t} I \times dt}{s} \quad (2)$$

where I (mA) is the applied discharging current, Δt (h) is the discharging time and S (cm^2) is the area of cell (1 cm^2).

The volume capacity (C_v, mAh cm^{-3}) was calculated from the discharge curve using the following equations:

$$C_V = \frac{\int_0^{\Delta t} I \times dt}{V} \quad (3)$$

where I (mA) is the applied discharging current, Δt (h) is the discharging time and V (cm^3) is the volume of the single cathode (0.036 cm^3) and the whole cell (0.083 cm^3). The specific energy density E_m (Wh kg^{-1}), E_v (Wh cm^{-3}) and specific power density P_m (kW kg^{-1}) of the Zn-PANAC batteries

$$E_m = C_m \times \Delta V \quad (4)$$

$$E_V = C_V \times \Delta V \quad (5)$$

$$P = \frac{C_m \times \Delta V}{1000 \times \Delta t} \quad (6)$$

Where the C_m and C_v are specific capacity and volume capacity, ΔV is the average discharge voltage and Δt (h) is the discharge time of the Zn-PANAC battery.

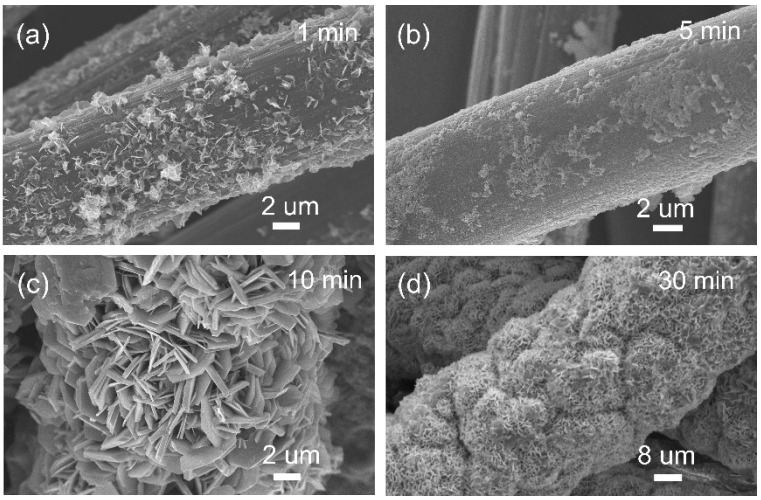

Fig. S1. SEM images of the CC@Zn NP electrode with different deposition time. (a) 1 min, (b) 5 min, (c) 10 min and (d) 30 min.

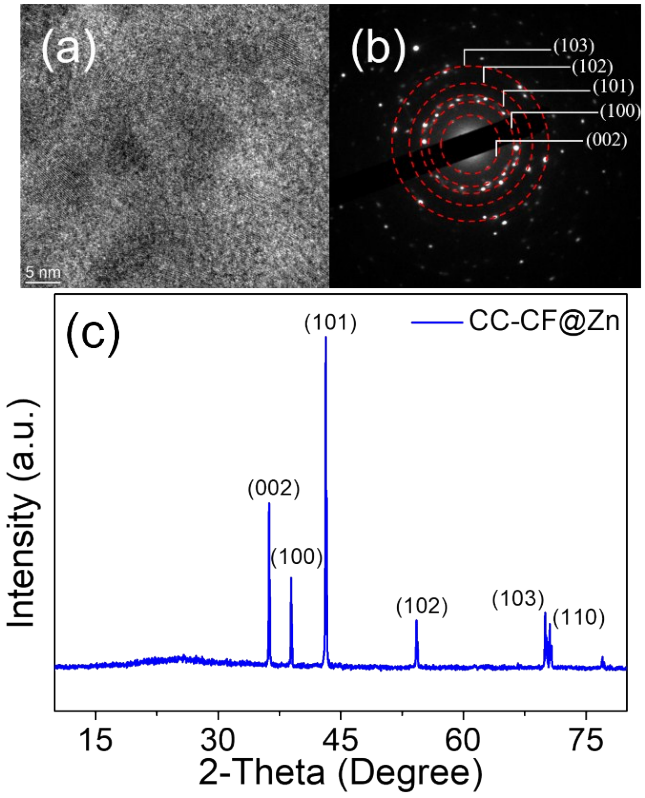

Fig. S2. (a) The high-resolution TEM image and (b) corresponding selected area electron diffraction of Zn nanoplates in CC@Zn NP anode. (c) XRD profile of the CC@Zn NP anode.

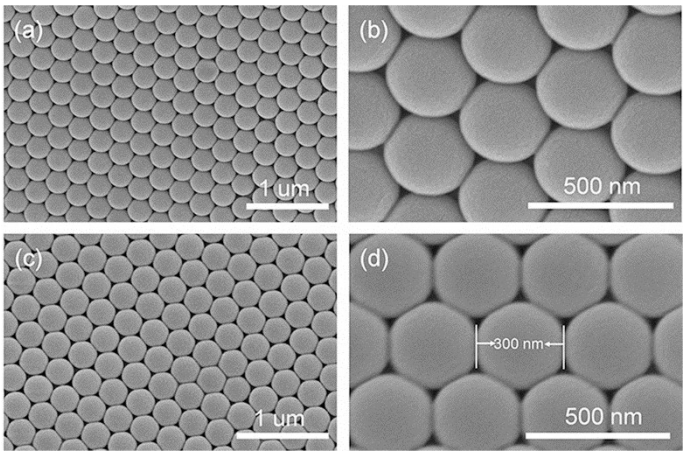

Fig. S3. (a, c) Low- and (b, d) high-magnification SEM images of PS-COOH spheres.

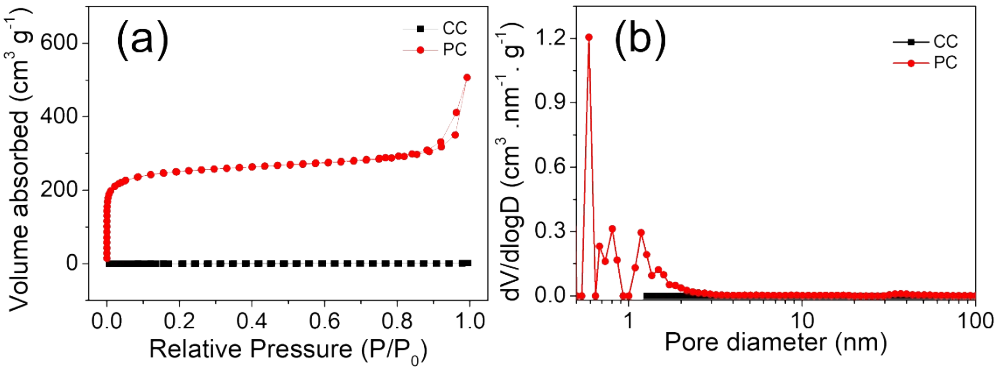

Fig. S4. (a) Nitrogen adsorption-desorption isotherms and (b) the corresponding pore size distribution curves of CC and PC.

We performed N_2 sorption measurements to investigate the texture property of CC-PC. As shown in Fig. S4, PC yields a specific surface area (SAA) of 948.9 $m^2 g^{-1}$, which is much larger than CC (1.4 $m^2 g^{-1}$). PC possesses predominant micropores and a few mesopores. In addition, there are plentiful periodic macropores with an average pore size of 300 nm in PC (see Fig. 1c in the main text). Therefore, for CC-PC composite, CC mainly serves as a flexible substrate while the coated PC functions as excellent conductive scaffold with hierarchical porous structure and high surface area which is beneficial to the ion diffusion and exposure of active sites.

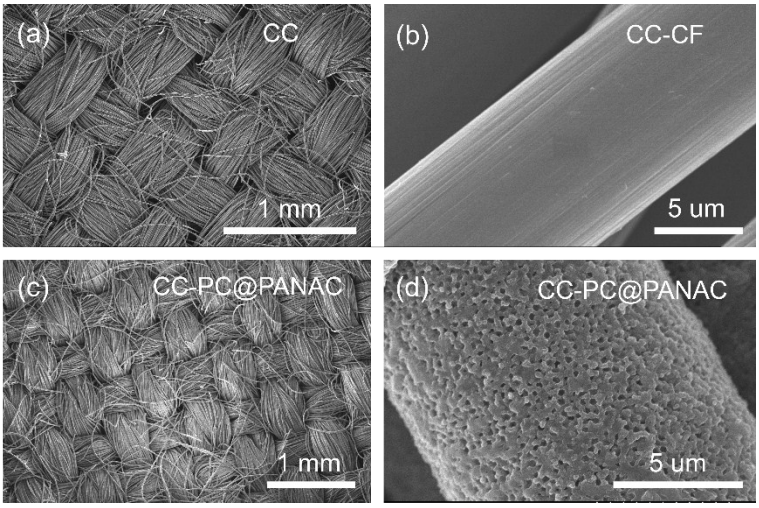

Fig. S5. (a-b) SEM images of CC and individual carbon fiber. (c-d) SEM images of CC-PC@PANAC.

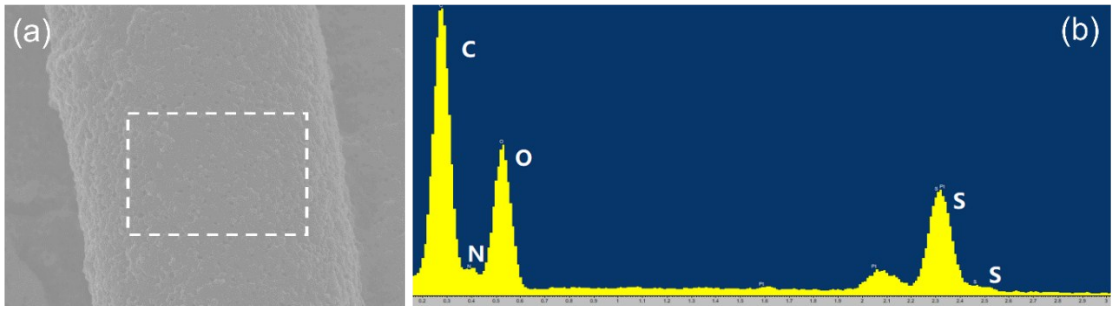

Fig. S6. SEM image and EDX spectrum of CC-PC@PANAC electrode.

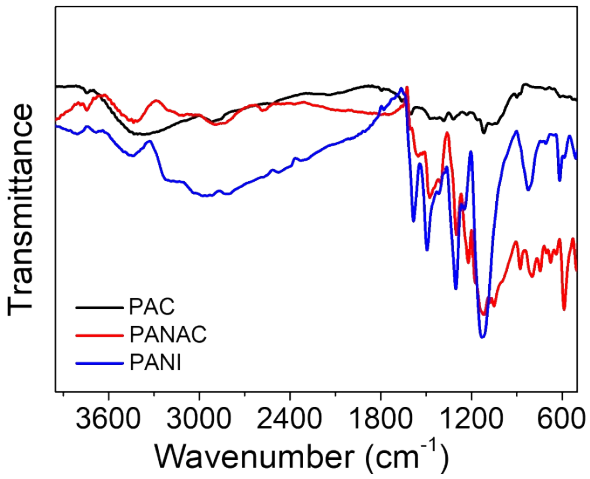

Fig. S7. FT-IR spectra of PAC, PANI and PANAC.

The PANAC cathode was characterized by Fourier transform infrared spectra (FTIR) with the parent PANI as a reference (Fig. S7). Clearly, the FTIR plot of the PANAC copolymer is analogous to that of the parent PANI to some extent and contains multiple characteristic bands,[3] *e. g.* the signals at 3224, 1584, 1494 cm^{-1} corresponding to the N−H stretching vibration of secondary amine, the C=N stretching of quinoid (Q) ring and the C−N stretching of benzenoid (B) ring, respectively. Noteworthy, the peak shift from 3224 cm^{-1} of PANI to 3203 cm^{-1} of PANAC is observed, manifesting the copolymer growth through the amino groups.[3] Compared to PANI, PANAC exhibits several new bands at 2900 (asymmetric C−H stretching of methyl groups in AC units), 2832 (symmetric C−H stretching of methyl groups), 1527 (N-H bending in secondary amine and C-N stretching in Q=N−B units), 1445 (C=N stretching of phenothiazine ring), 1162 cm^{-1} (the C−H in-plane binding vibration of phenothiazine ring), respectively.[3] Furthermore, another three new peaks at 1079, 1052 and 1003 cm^{-1} (in-plane C−H bending) are attributed to the incorporation of phenothiazine ring into the copolymer chain, while five peaks at 660-

1000 cm^{-1} are assigned to the out-of-plane C−H bending.[4] In particularly, the new peak at 876 cm^{-1} in PANAC represents the AC unit are ortho-coupled, because the AC monomer both exist at least one primary amino group and at least non-substituted ortho position which is similar to that of polythionine[5,6] and poly(o-phenylenediamine)[7]. The above results confirm the successful copolymerization of aniline and AC. It is noted that the appearance of the 1120 cm^{-1} band for PANAC comes from the sulfate dopant as counter ions to neutralize the positive charge,[8] since the copolymerization of aniline and AC was performed in H_2SO_4. The FT-IR spectrum of PANAC is different from PAC (Fig. S7). From the above results, we can see that the shape of the FTIR spectrum of PANAC is not a simple superposition of the shape of the spectrum of PANI and PAC and is more like the shape of the spectrum of PANI, indicating the PANAC is a copolymer and the aniline units dominant the chain of PANAC rather than the AC units.[5-7]

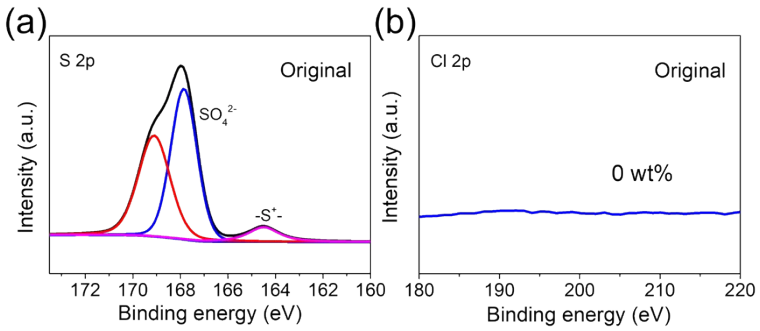

Fig. S8. XPS S 2p (a) and Cl 2p (b) spectra of CC-PC@PANAC cathode at the original, state.

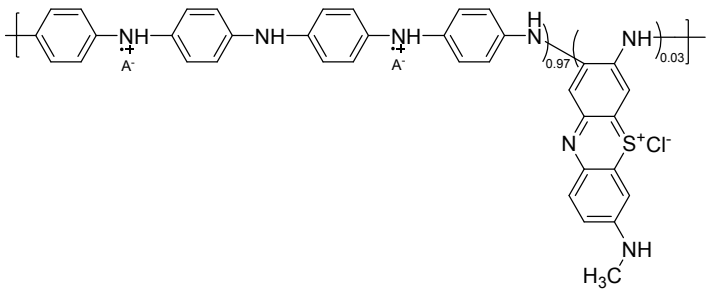

Fig. S9. Schematic representation of the possible chemical structure of PANAC.

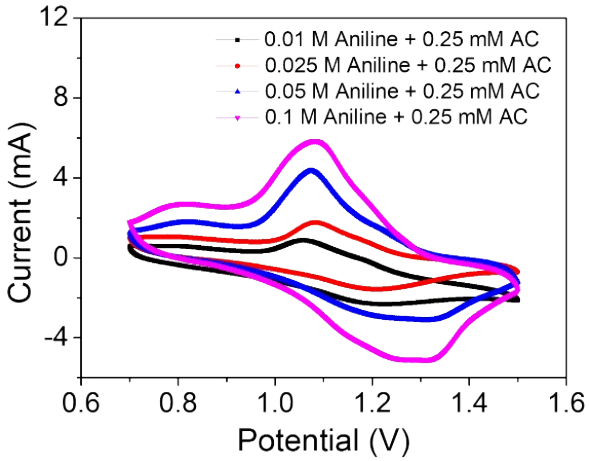

Fig. S10. CV curves of CC-PC@PANAC electrode at different aniline/AC ratios in aqueous Zn-PANAC rechargeable battery at the scan rate of 1 mV s^{-1}.

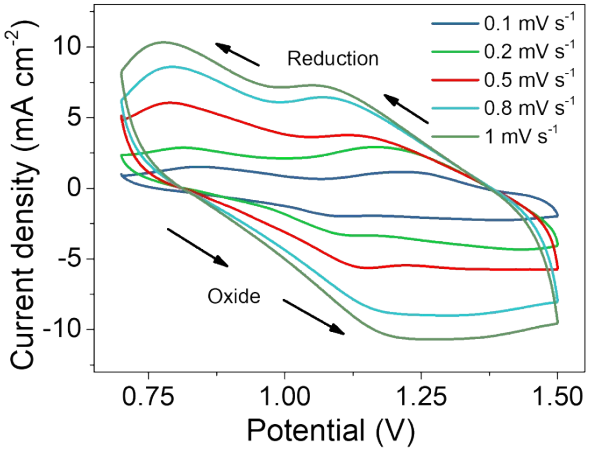

Fig. S11. CV curves of the CC-PC@PANAC electrode at different scan rates in aqueous Zn-PANAC rechargeable battery.

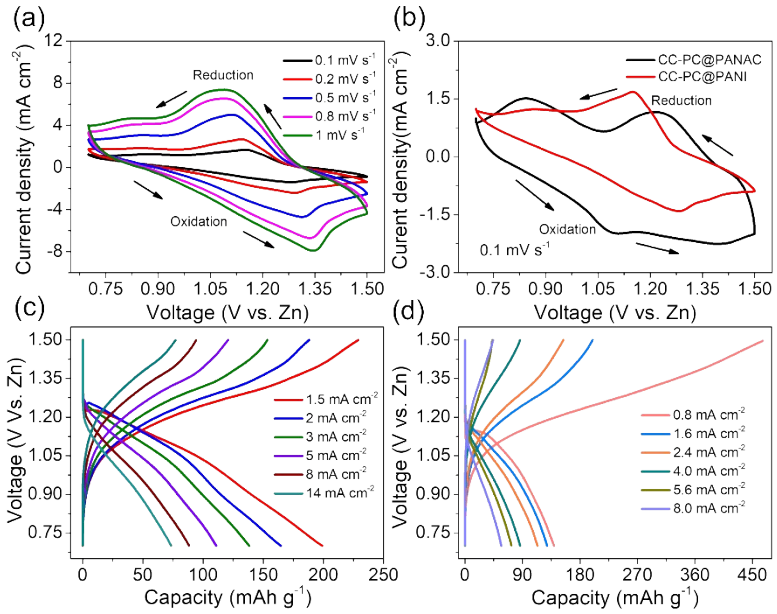

Fig. S12. (a) CV curves of the CC-PC@PANI cathode at different scan rates, comparative CV (b) of aqueous rechargeable zinc batteries using CC-PC@PANAC and CC-PC@PANI as the cathodes. (c-d) Galvanostatic charge-discharge curves of aqueous rechargeable zinc batteries using CC-PC@PANI (c) and CC@PANI cathode (d), respectively.

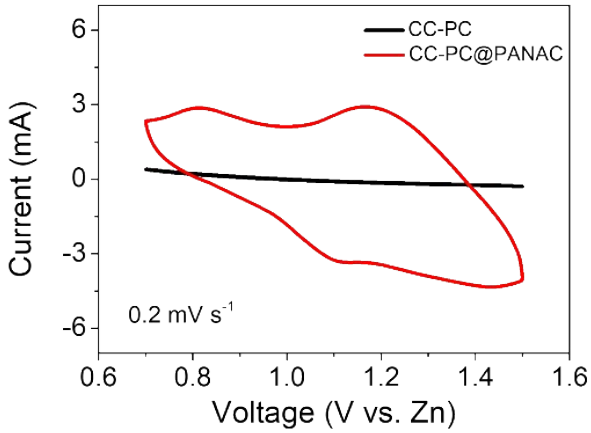

Fig. S13. Comparative CV curves of CC-PC and CC-PC@PANAC cathodes.

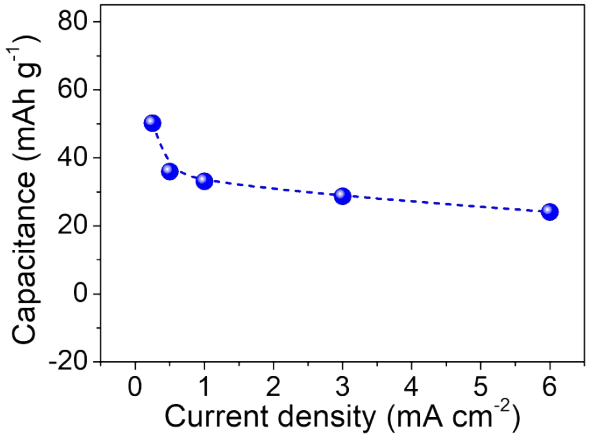

Fig. S14. Specific capacity as a function of current density of aqueous Zn–PAC batteries at pH=5.

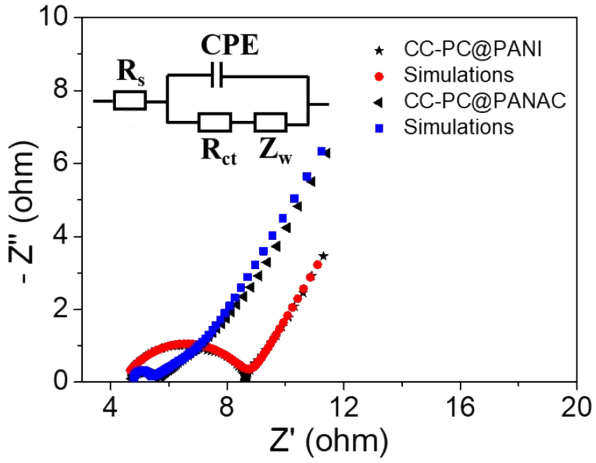

Fig. S15. Experimental and fitting Nyquist plots of aqueous rechargeable zinc batteries with CC-PC@PANI and CC-PC@PANAC cathodes. The inset is equivalent circuit diagram for two kinds of batteries.

Fig. S15 exhibits the Nyquist plots of various electrodes. Apparently, the PANAC electrode shows similar series resistance but markedly lower charge transfer resistance (R_{ct} = 0.8 Ω) with respect to PANI (R_{ct} = 4.1 Ω), implying drastically-enhanced charge-transfer rate and much higher redox activity of PANAC.

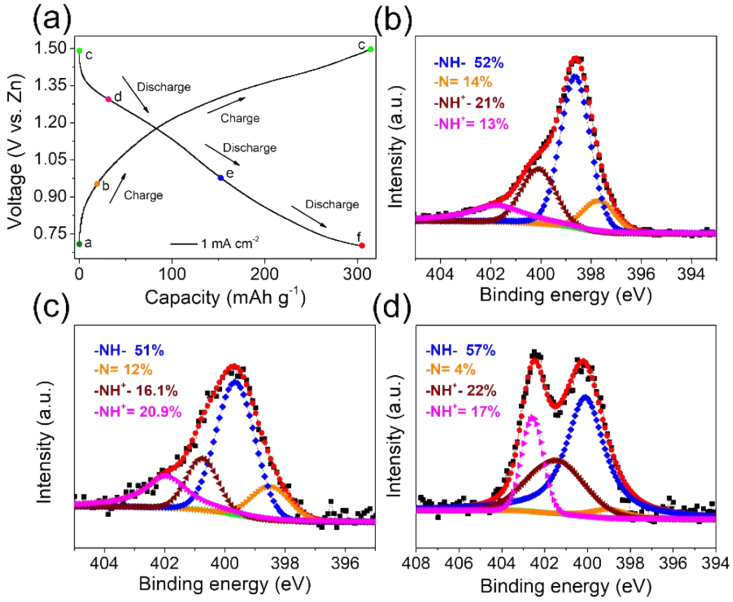

Fig. S16. (a) The charge-discharge curves of Zn-PANAC batteries at a current density of 1 mA cm^{-2}. XPS N 1s spectrum of CC-PC@PANAC cathode at different charged and discharged states: (b), (c) and (d) correspond to point b, d and e in (a), respectively.

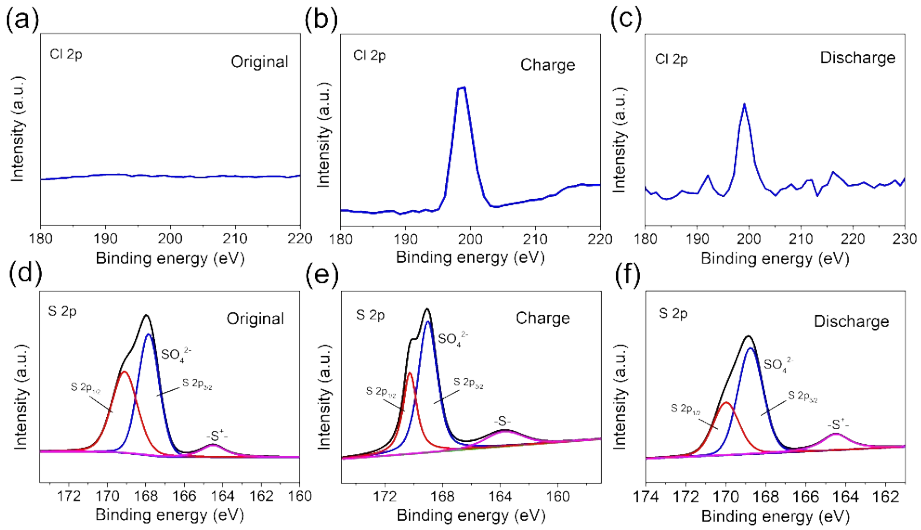

Fig. S17. XPS Cl 2p and S 2p spectra of CC-PC@PANAC cathode at the original, charged, and discharged states. Upon the discharge, the PANAC was reduced along with the significant reduction of the Cl^- dopant from 16.9 at % to 3.2 at %.

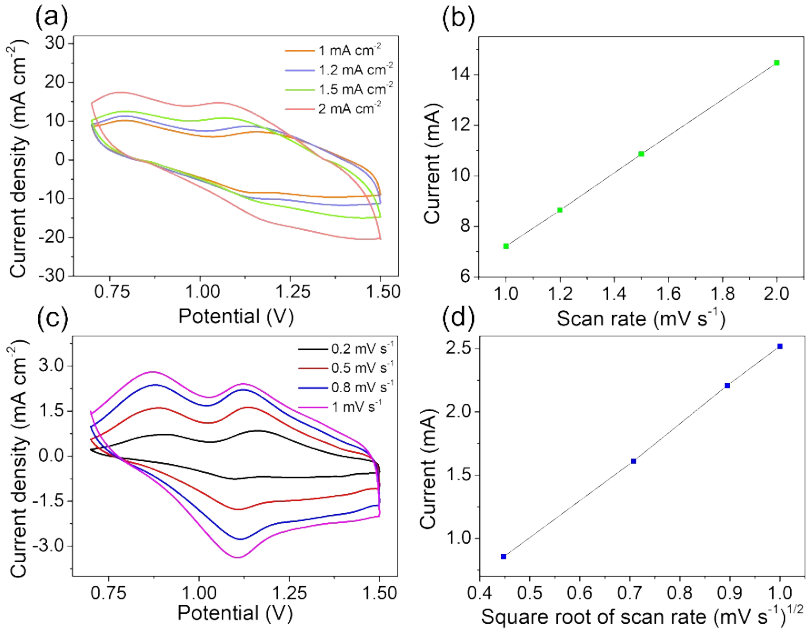

Fig. S18. (a) CV curves of CC-PC@PANAC electrode at different scan rates. (b) Current response at the cathode peak vs. the scan rate (y = 7.254x-0.04159, R^2 = 0.9999) of CC-PC@PANAC electrode. (c) CV curves of Pt plate@PANAC electrode at different scan rates. (d) Current response at the cathode peak vs. the square root of scan rate (y = 3.027x-0.509, R^2 = 0.9994) of Pt plate@PANAC electrode.

We recorded CV curves of two electrodes at different scan rates. As seen in Fig. S18, the cathodic peak current for CC-PC@PANAC shows a linear increase with

increasing scan rate. In contrast, the peak current of Pt-plate@PANAC increases linearly with an increase in the square root of scan rate. The contributions of surface reactions at different voltages can be assessed on the basis of the equation of $i = av^b$, where b ranges from 0.5 to 1, representing the reactions from bulk to the surface and/or near-surface.[9] CC-PC@PANAC gives a much higher b value (b = 1) than that of Pt-plate@PANAC (b = 0.5), indicating a dominant fraction of contributions from surface reactions during the charge-discharge process, leading to the rapid kinetics of cells.

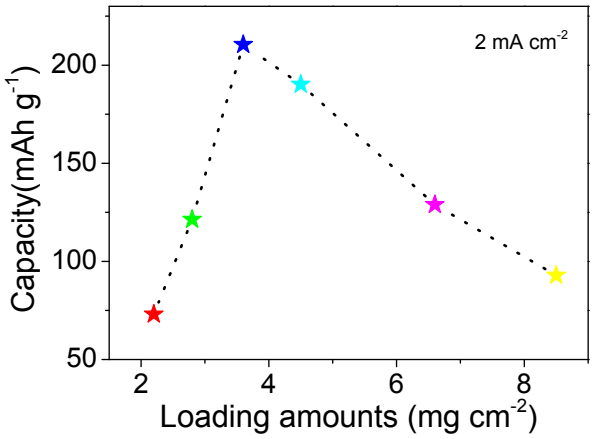

Fig. S19. Plots of specific capacity of aqueous Zn-PANAC battery *versus* the different mass loading**.** It is noted that the optimal performance corresponds to a mass loading of ~3.6 mg cm^{-2}.

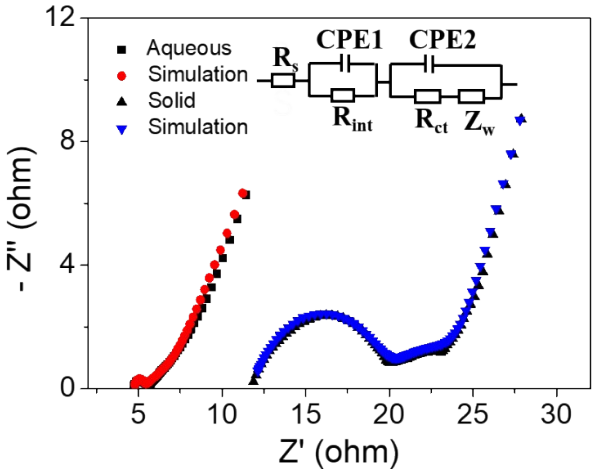

Fig. S20. Experimental and fitting Nyquist plots of aqueous and quasi-solid-state Zn-PANAC batteries. The inset is used equivalent circuit diagram for quasi-solid-state Zn-PANAC batteries. The used equivalent circuit diagram for aqueous Zn-PANAC batteries is presented in inset of Fig. S15.

The Nyquist plot of quasi-solid-state Zn-PANAC batteries consists of two semicircles in high and medium frequency regions respectively, and a straight slopping line at the low frequency region. The first semicircle at the high frequency region is probably derived from the interfacial contact resistance (R_{int}) between the gel electrolyte and solid electrodes, while CPE1 represent its related double layer capacitance.[10-13] The second circle at the medium-frequency region represents the charge transfer resistance (R_{ct}) and its related double layer capacitance (CPE2).[10-13] The straight slopping line is attributed to the diffusion process in electrodes.

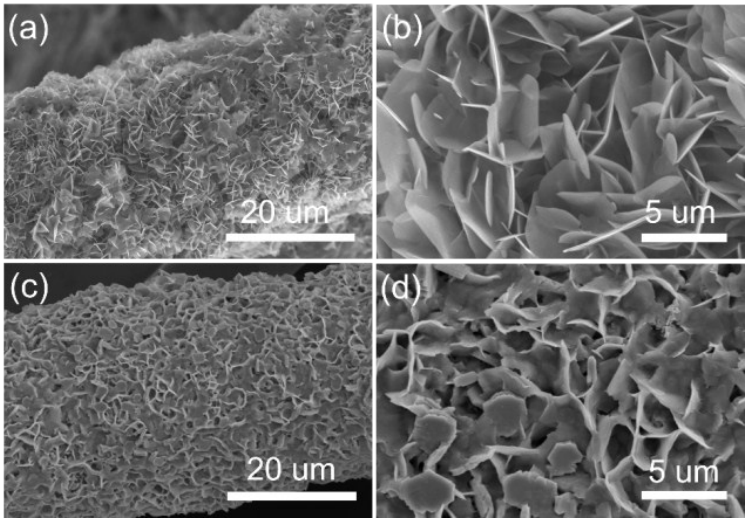

Fig. S21. SEM images of CC@Zn NP anode: (a-b) before cycling test. (c-d) after cycling test.

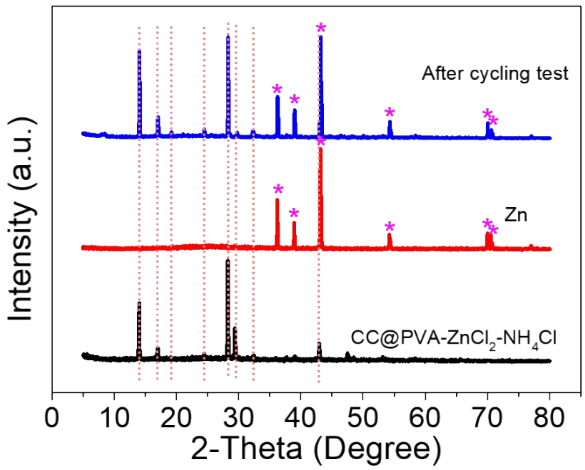

Fig. S22. The XRD pattern of the CC@Zn NP anode before and after cycling test as well as CC@PVA/$ZnCl_2$-NH_4Cl

It is worthy to note that the cycle stability of our quasi-solid-state Zn-PANAC battery is tested in the PVA/$ZnCl_2$-NH_4Cl gel electrolyte. In order to maintain the structure of the Zn nanosheets of CC@Zn NP anode after cycling test, we directly measured the dried post-test electrode without any other treatment. As can be seen from Fig. S22, the XRD peaks for the CC@Zn NP anode prior to cycling tests are attributed to the Zn nanoplates. After cycling tests in gel electrolytes, the XRD peaks

of the Zn nanoplate still exist and the newly appeared XRD peaks come from the PVA/$ZnCl_2$-NH_4Cl electrolyte (Fig. S22). Of note, no other new XRD peaks are observed after cycling tests (Fig. S22), suggesting the absence of Zn-related compounds (e.g. ZnO et al) at the cycled CC@Zn NP anode. In addition, SEM images shown in Fig. S21 indicate that the Zn nanoplate still maintains sheet-like morphology. Similar with some previous reports,[14, 15] the observed wrinkles could be mainly attributed to the coating of the PVA polymer, since the cycling stability test is performed in PVA/$ZnCl_2$-NH_4Cl gel electrolyte.

Table S1. Comparison of the specific capacity of our Zn-PANAC battery with selective recently-reported aqueous Zn batteries with various conductive polymer cathodes

Cathode	Electrolyte	Capacity (mAh g^{-1})	Reference
PANAC	**2 M $ZnCl_2$, 3 M NH_4Cl at pH 5**	**306.3 (1 mA cm^{-2})**	**This work**
self-doped PANI	1 M $ZnSO_4$	184 (0.2 A g^{-1})	*Angew. Chem. Int. Ed.* **2018**, *130*, 16597.
PANI	$Zn(CF_3SO_3)_2$	200	*Adv. Funct. Mater.* **2018**, *28, 1804975*
PANI	1 M $ZnCl_2$	162 (1 C)	*ACS Nano* **2018**, *DOI: 10.1021/acsnano.8b02744.*
PANI with 4,4-diaminobiphenyl	1 M $ZnSO_4$, 0.3 M $(NH_4)_2SO_4$	183.28 (2.5 mA cm^{-2})	*J. Power Sources* **2015**, *283*, 125.
PANI	1 M NH_4Cl, 0.5 M $ZnCl_2$	139.4-170.1 (0.02 mA cm^{-2})	*Electrochim. Acta* **2009**, *54*, 2941.
self-doped PANI	1 M $ZnCl_2$, 0.5 M NH_4Cl	146.4	*J. Power Sources* **2002**, *110*, 229.
poly(aniline-co-N-methylthionine)	2 M $ZnCl_2$, 3 M NH_4Cl	146.3 (1 mA cm^{-2})	*Electrochim. Acta* **2016**, *190*, 240.
PANI/graphite	1 M $ZnCl_2$, 0.5 M NH_4Cl	142.2 (0.6 mA cm^{-2})	*J. Power Sources* **2007**, *170*,153.
PANI	2 M $ZnCl_2$, 3 M NH_4Cl	141.2 (0.5 mA cm^{-2})	*Synthetic Met*. **2008**, *158*, 242.
poly(aniline-co-m-aminophenol)	2 M $ZnCl_2$, 3 M NH_4Cl	137.5 (0.5 mA cm^{-2})	*J. Power Sources* **2006**, *161*, 685.
PANI	0.2 M $ZnCl_2$, 0.50 M NH_4Cl with 0.33 M Na-citrate	130 (0.25 mA cm^{-2})	*J. Power Sources* **2006**, *160*, 1447.
PANI	0.5 M NH_4Cl, 0.2 M $ZnCl_2$	109.5 (0.05 A g^{-1})	*Int. J. Electrochem. Sci.* **2016**, 11, 8571.
poly(aniline-co-o-	2.5 M $ZnCl_2$, 3 M NH_4Cl	103.0 (0.5 mA cm^{-2})	*Synthetic Met*. **2014**, *143*, 269.

aminophenol
)

Table S2. The comparison of the electrochemical performance of our Zn-PANAC cell with selective recently-reported aqueous batteries.

Battery	Capacity (mAh g^{-1})	Energy density (Wh kg^{-1})	Cycle	Reference
Zn-PANAC	306.32	352.3	1100	**This work**
Zn-ion	300	250	1000	*Nat. Energy* **2016**, *1*, 16119.
Zn-PANI	184	*56	2000	*Angew. Chem. Int. Ed.* **2018**, *130,* 16597.
Zn-MnO_2	210	/	100	*Angew. Chem. Int. Ed.* **2012**, *124,* 957.
Zn-PANI	200	/	3000	*Adv. Funct. Mater.* **2018**, *28*, 1804975.
Zn-PANI	162	/	100	*ACS Nano* **2018**, *12,* 11838
Zn-V_2O_5	372	*144	900	*Adv. Mater.* **2018**, *30*, 1703725
Zn-pyrene-4,5,9,10-tetraone (PTO)	336	186.7	1000	*Angew. Chem. Int. Ed.* **2018**, *130*, 11911.
Ni-Fe	126	141	800	*Nat. Commun*. **2012**, *3*, 917.
Ni-Fe	118	*100.7	1000	*Nano Lett*. **2014**, *14*, 7180.
Ni-Fe	81	/	100	*Chem. Commun*. **2011**, *47*, 12473.
Ni-Zn	203	355.7	/	*Adv. Mater*. **2016**, *28*, 8732.
Ni-Zn (Zn//Co_3O_4@NiO)	182.6	215.51	500	*Inorg. Chem. Front*. **2015**, *2*, 184.
Ni-Zn (Zn//NiO)	155	228	500	*J. Mater. Chem. A* **2015**, *3*, 8280.
Ni-Zn (Zn//Ni_3S_2)	148	/	100	*ACS Appl. Mater. Interfaces* **2015**,

				7, 26396.
Zn-Co_3O_4	162	241	2000	*Adv. Mater.* **2016**, *28*, 4904.
Ni-Bi	113	92	80	*J. Power Sources* **2015**, *274*, 1070.
Ni-Bi	57.2	85.8	90	*Adv. Mater*. **2016**, *28*, 9188.
Li-ion ($Na_2V_6O_{16}\cdot 14H_2O$//$LiMn_2O_4$)	122.7	/	200	*J. Power Sources* **2013**, *227*, 111.
TiO_2//$Ni(OH)_2$	68.7	/	100	*Energy Environ. Sci*. **2010**, *3*, 1732.

Note: *represents the energy density calculated based on the total mass of two electrodes and electrolytes.

Table S3. The calculated contents of various N species of the CC-PC@PANAC cathode under different charging and discharging states in Fig. S16.

Sample	Calculated contents of various N species (%)			
	-N=	-NH-	$-NH^+-$	$-NH^+=$
a	13.5	57.5	18.8	10.2
b	14	52	21	13
c	12.5	46.4	9.8	31.2
d	12	51	16.1	20.9
e	4	57	22	17
f	2	91	7	0

Reference

1. Z. Deng, H. Jiang, Y. Hu, Y. Liu, L. Zhang, H. Liu and C. Li, *Advanced Materials*, 2017, **29**, 1603020.
2. J. Liu, C. Guan, C. Zhou, Z. Fan, Q. Ke, G. Zhang, C. Liu and J. Wang, *Advanced materials*, 2016, **28**, 8732-8739.
3. L. Xiao, Y. Cao, J. Xiao, B. Schwenzer, M. H. Engelhard, L. V. Saraf, Z. Nie, G. J. Exarhos and J. Liu, *Advanced materials*, 2012, **24**, 1176-1181.
4. A. Kellenberger, E. Dmitrieva and L. Dunsch, *Physical Chemistry Chemical Physics*, 2011, **13**, 3411-3420.
5. D. D. Schlereth and A. A. Karyakin, *Journal of Electroanalytical Chemistry*, 1995, **395**, 221-232.
6. R. Yang, C. Ruan, W. Dai, J. Deng and J. Kong, *Electrochimica Acta*, 1999, **44**, 1585-1596.
7. S. Sivakkumar and R. Saraswathi, *Journal of applied electrochemistry*, 2004, **34**, 1147-1152.
8. H. Y. Shi, Y. J. Ye, K. Liu, Y. Song and X. Sun, *Angewandte Chemie*, 2018, **130**, 16597-16601.
9. Y. Kong and S.-L. Mu, *Acta. Phys.-Chim. Sin.,* 2001, **17**, 295-299.
10. Y. T. Li, X. Chen, A. Dolocan, Z. M. Cui, S. Xin, L. G. Xue, H. H. Xu, K. Park and J. B. Goodenough, *J. Am. Chem. Soc.*, 2018, **140**, 6448-6455.
11. F. Orsini, M. Dolle´ and J.-M. Tarascon, *Solid State Ionics*, 2000, **135**, 213-221.
12. Q. S. Wang, Z. Y. Wen, J. Jin, J. Guo, X. Huang, J. H. Yang and C. H. Chen, *Chem. Commun.,* 2016, **52**, 1637-1640.
13. F. R. Qin, K. Zhang, J. Fang and Y. Q. Lai, Q. Li, Z. Zhang and J. Li, *New J. Chem.,* 2014, **38**, 4549-4554.
14. Q. Wu, J. Zhang and S. Sang, *J. Phys. Chem. Solids*, 2008, **69**, 2691-2695.
15. Y. X. Zeng, X. Y. Zhang, Y. Meng, M. H. Yu, J. N. Yi, Y. Q. Wu, X. H. Lu and Y. X. Tong, *Adv. Mater.,* 2017, **29**, 1700274.